J Intell Robot Syst (2016) 83:271–288
DOI 10.1007/s10846-015-0311-2

Experimental Analysis of Variable Collective-pitch Rotor Systems for Multirotor Helicopter Applications

Robert Porter · Bijan Shirinzadeh · Man Ho Choi

Received: 15 March 2015 / Accepted: 16 November 2015 / Published online: 19 November 2015

Abstract This paper presents an experimental study of variable collective-pitch rotor systems for multirotor helicopter applications. An experimental research facility has been established to conduct this research. The facility enables the high-resolution measurement of forces and torques produced by rotor systems. The power consumption of the rotor system during experimentation can also be recorded. The experimental research facility also allows for the characterisation of the effect of rotor systems on multirotor helicopter performance. It is shown that the variable collective-pitch rotors have a significant performance advantage over fixed-pitch rotors when comparing thrust response, and multirotor helicopter step input response performance. Further, it is observed that variable collective-pitch rotors are more efficient in terms of energy consumption than comparable fixed-pitch rotors under similar operating conditions.

Keywords Unmanned aerial vehicle · Multirotor helicopter · Variable collective-pitch rotor · Experimental analysis

R. Porter (✉) · B. Shirinzadeh · M. H. Choi
Robotics and Mechatronics Research Laboratory, Monash University, Wellington Road, Clayton, Victoria, Australia
e-mail: robert.porter@monash.edu

1 Introduction

Unmanned Aerial Vehicles (UAVs) have received widespread attention in both military and civilian domains in recent years [2, 21, 26]. In particular, multirotor helicopters have been the subject of significant research since gaining attention in the early 2000s [5, 11, 13, 25, 27]. Applications for multirotor helicopter research range from data collection and surveillance [15], to cleaning up after nuclear waste spills [13]. Much of this research has been focused on the control aspect of multirotor helicopters [6, 18]. To this end, most research groups have chosen to modify commercially available hobbyist systems [20, 22, 24].

The increased research efforts into multirotor helicopters are primarily due to the robustness and mechanical simplicity of the multirotor helicopter platform [11, 23]. Traditional pod-and-boom helicopters make use of swashplates to alter the cyclic and collective rotor pitch to affect changes in thrust, and rolling and pitching moments. The incorporation of swashplates significantly increases the mechanical complexity of the system. Multirotor helicopters are able to affect rolling and pitching motions by utilising multiple rotors to generate thrust differentials across the body of the aircraft. This removes the necessity of the swashplate. The mechanical complexity of multirotor helicopters is further reduced by the utilisation of rotors that also have fixed collective-pitch.

To vary the thrust produced by fixed-pitch rotors, the angular velocity of the rotors must be changed. This places fundamental constraints on the flight envelopes of multirotor helicopters. In particular, the response time of the rotor is limited by the rotational moment of inertia of the motor-rotor pair. Experimental studies have demonstrated that thrust rise times of $> 0.2s$ render multirotor helicopters uncontrollable [23]. For small multirotor helicopters, $< 4kg$, the motors and rotors are not required to be sufficiently large to increase thrust rise times above this threshold.

However, heavier multirotor helicopters require larger rotors [16]. The torque required to rapidly change the angular velocity of large rotors quickly surpasses the torque that can be supplied by motors suitable for multirotor applications. This limitation effectively constrains the maximum size of multirotor helicopters.

Although stable flight control of small multirotor helicopters equipped with fixed-pitch rotors can be achieved, traditional helicopters have demonstrated aggressive flight manoeuvres outside of the flight envelope of multirotor helicopters [1, 12]. This is in part due to the ability of traditional helicopters to produce reverse thrust, allowing for inverted flight manoeuvres and sudden changes in direction. Enabling the performance of these types of manoeuvres for multirotor helicopters would significantly increase the number of potential applications for this type of aircraft, particularly in cluttered environments.

To overcome the limitations of fixed-pitch rotors, the implementation of variable collective-pitch rotors for multirotor helicopter applications has been suggested in the literature [4, 11]. The consensus among these researchers is that adding variable collective-pitch rotors - without incorporating a swashplate to any of the rotors - does not significantly increase the mechanical complexity of the aircraft design, nor does it reduce its robustness. In [11], the authors demonstrated agile flight manoeuvres using a feed-forward variable collective-pitch actuator model. A computational analysis of the dynamic performance of fixed and variable collective-pitch rotors was also performed. However, limited effort has been made to experimentally verify the extended control bandwidth of variable-pitch rotors for multirotor helicopter application or to investigate the effect of rotor angular velocity on the control bandwidth of multirotor helicopters.

A further consideration for rotors for multirotor helicopter application is the effect they have on the power consumption of the system. A critical design consideration for all aircraft is their weight. As aircraft must carry a power supply on board, the amount of energy the system consumes during flight is an important specification. This is especially true of multirotor helicopters, which do not have passive lifting surfaces and must provide thrust to overcome the weight of the system. An investigation into the performance of variable collective-pitch rotor systems with respect to power consumption is therefore necessary.

The remainder of this paper is organised as follows. In Section 2 the dynamics models of electric motors, and variable collective-pitch rotors are presented. Section 2 also includes a discussion of methods of control allocation for variable-pitch rotor systems. The experimental methodology and analysis of the dynamic response and power consumption of variable collective-pitch rotors is presented in Section 3. In Section 4, the effects of actuator control bandwidth on the flight performance of a multirotor helicopter is experimentally determined. The effects of actuator selection on power consumption of the multirotor helicopter are also characterised. A computational analysis is conducted in Section 5 to further explore the flight performance of variable collective-pitch rotor-equipped multirotor helicopters. Finally, conclusions are drawn in Section 6.

2 Thrust Actuation

2.1 Rotor Aerodynamics Model

To determine the dynamics model of variable collective-pitch rotors, it is necessary to undertake a detailed study of rotor aerodynamics. The rotors used in this experimental analysis are symmetric, almost rectangular, and have a radius of $125mm$. As the maximum chord-to-thickness ratio of the rotor blades is 12 %, a NACA 0012 airfoil is chosen to model the rotor blades. It is assumed that the flow is laminar over the rotor blade.

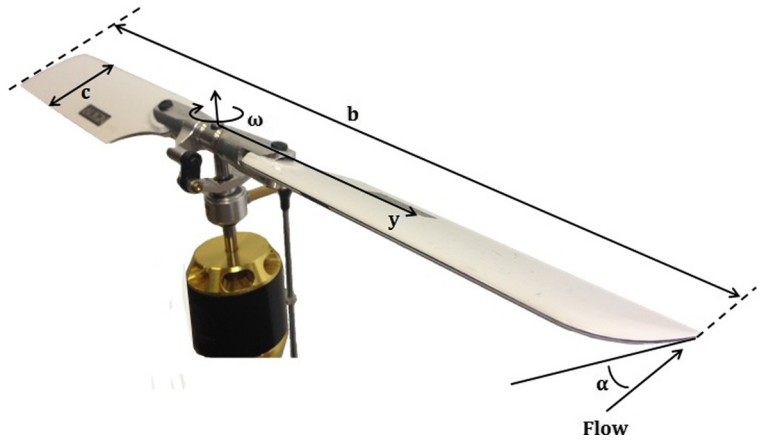

Fig. 1 The variable collective-pitch rotor

Due to the symmetry and low thickness-to-chord ratio of the rotor blade, the infinite-blade sectional lift coefficient, c_l, is given by [14]

$$c_l = 2\pi\alpha \equiv m_o\alpha, \tag{1}$$

where α is the local angle of attack, as shown in Fig. 1.

To correct for the finite rotor blade, it is necessary to calculate the sectional lift coefficient considering the flow field around the finite wing. The following change of coordinates is made

$$\theta = \cos^{-1}(\frac{2y}{b}), \tag{2}$$

where b is the length of the rotor blade, and y is the position along the blade measured from the plane of symmetry. b and y are labelled in Fig. 1.

For an arbitrary circulation distribution, the sectional lift coefficient is given by [14]

$$c_l = \frac{m_{o_s}c_s}{c}\sum_{n=1}^{\infty} A_n \sin(n\theta), \tag{3}$$

where c is the local rotor blade chord length shown in Fig. 1, the subscript s refers to the values at the plane of symmetry, and the values of A_n can be found by solving the Eq. 4 at N *stations* along the rotor blade. In Eq. 4, α_a is the absolute angle of attack, and the true values of A_n are found in the limit as $N \to \infty$.

$$\alpha_a(\theta) = \frac{m_{o_s}c_s}{m_o c}\sum_{n=1}^{N} A_n \sin(n\theta) + \frac{m_{o_s}c_s}{4b}\sum_{n=1}^{N} nA_n \frac{\sin(n\theta)}{sin\theta} \tag{4}$$

For the non-cambered, almost rectangular, rotor blade in question, it can be assumed that α_a is equal to α everywhere along the span, and that $c = c_s$ and $m = m_o$. Therefore, Eq. 4 is simplified to

$$\alpha = \sum_{n=1}^{N} A_n \sin(n\theta)(1 + \frac{n\pi}{2\mathcal{A}\sin\theta}), \tag{5}$$

where $\mathcal{A}$ is the aspect ratio of the rotor blade. Equation (5) can be solved simultaneously for A_n. The coefficient of the total lift of the rotor blade is given by the weighted integral of Eq. 3:

$$C_L = \int_{-b/2}^{b/2} \frac{c_l q_\infty c}{q_\infty S} dy = \frac{\pi m_{o_s} c_s b}{4S} A_1, \tag{6}$$

where S is the wing area, and q_∞ is the dynamic pressure of the local flow.

The coefficient of total induced drag on the rotor blade, C_{D_i}, can then be calculated using the following:

$$C_{D_i} = (C_{D_i})_{el}\sum_{n=1}^{N} \frac{nA_n^2}{A_1^2}, \tag{7}$$

where $(C_{D_i})_{el}$ is the coefficient of total induced drag on the rotor blade for an elliptical lift distribution, and is calculated as

$$(C_{D_i})_{el} = \frac{C_L^2}{\pi\mathcal{A}}. \tag{8}$$

Making the assumption that the flow into the rotor is uniform, the coefficient of total thrust of the rotor, C_T, can then be calculated as using Eq. 9 [16].

$$C_T = \frac{1}{2}\sigma B^2 C_{L_\alpha}(\frac{\alpha_0 B}{3} - \frac{\lambda}{2}) \tag{9}$$

Table 1 Analytic rotor blade aerodynamic coefficients

C_{L_α}	C_{L_0}	C_{D_i}	C_{D_0}
2.44	0.0	$0.23\alpha^2$	0.01

In Eq. 9 σ is the ratio of the rotor blade area to the area of the total disk swept by the rotor, B is a tip-loss correction factor, C_{L_α} is the derivative of the total lift coefficient of the rotor blade with respect to α, α_0 is the angle of attack of the rotor blade at the root of the rotor, and λ is the dimensionless inflow into the rotor and is given by

$$\lambda = \sqrt{\frac{C_T}{2}}. \tag{10}$$

Likewise, the coefficient of total torque of the rotor, C_Q, is calculated as

$$C_Q = \frac{1}{2}\sigma C_{L_\alpha}\kappa\lambda\left(\frac{\alpha_0}{3} - \frac{\lambda}{2}\right) + \frac{1}{8}\sigma C_D, \tag{11}$$

where κ is an induced power factor and includes the effects of both tip loss and nonuniform inflow, and C_D is the coefficient of total drag of the rotor blade and is calculated as follows,

$$C_D = C_{D_0} + C_{D_i}(\alpha_0), \tag{12}$$

where C_{D_0} is the zero rotor-angle coefficient of drag.

Using a simple momentum analysis, κ is approximately equal to 1.25 [16].

The theoretical aerodynamic coefficients obtained for the rotor blade are presented in Table 1.

2.2 Actuator Dynamics Model

Brushless DC motors are utilised to drive the rotors on board typical multirotor helicopters. The DC-motor is well modelled by a resistor, inductor and voltage generator in series [7]. For small DC motors the inductance term can be neglected as the response of the electrical part of the system is significantly faster than the mechanical part. Therefore, the following equation is adequate to describe the DC motor.

$$v = Ri + K_E\omega_M \tag{13}$$

In Eq. 13 v is the voltage applied to the motor, R is the resistance of the motor, i is the current through the motor, K_E is called the motor constant and ω_M is the angular velocity of the motor.

Further, the dynamics of the motor is described by the following equation

$$I_{TM}\dot{\omega}_M = Q_M - Q_L, \tag{14}$$

where I_{TM} is the total motor and motor load moment of inertia, $\dot{\omega}_M$ is the angular acceleration of the motor, Q_M is the motor torque, and Q_L is the load torque.

The motor torque, Q_M, is proportional to the electrical current, i, through constant K_M. Therefore, the dynamics of the motor can be written by combining Eqs. 13 and 14. The resulting differential equation is:

$$I_{TM}\dot{\omega}_M = -\frac{K_E K_M}{R}\omega_M + \frac{K_M}{R}v - Q_L. \tag{15}$$

Neglecting any friction inside the motor, the load torque can be calculated as the total torque due to the rotor,

$$Q_L = \rho A R^3 \omega^2 C_Q. \tag{16}$$

In Eq. 16, ρ is the density of air, A is the area swept out by the rotor, and R is the rotor radius.

Assuming that the inflow velocity, V_i, is approximately constant under multirotor operating conditions, the following approximation can be made [16]:

$$\lambda \approx \frac{V_i}{R\omega}. \tag{17}$$

Eq. 16 can therefore be simplified into an equation of the following form

$$Q_L = K_{Q_1}\omega^2\alpha_0^2 + K_{Q_2}\omega^2 + K_{Q_3}\omega\alpha_0 - K_{Q_4}, \tag{18}$$

where

$$\begin{aligned} K_{Q_1} &= \rho R^4 c C_{D_i} \\ K_{Q_2} &= \frac{1}{4}\rho R^4 c C_{D_0} \\ K_{Q_3} &= \rho R^3 c\kappa V_i C_{L_\alpha} \\ K_{Q_4} &= \frac{1}{2}\rho R^2 c\kappa V_i^2 C_{L_\alpha}. \end{aligned} \tag{19}$$

Substituting Eq. 18 into Eq. 15 results in the following nonlinear actuator dynamics model

$$\begin{aligned} I_{TM}\dot{\omega} = &-K_{M_1}\omega + K_{M_2}v - K_{Q_1}\omega^2\alpha_0^2 \\ &-K_{Q_2}\omega^2 - K_{Q_3}\omega\alpha_0 + K_{Q_4}, \end{aligned} \tag{20}$$

where

$$\begin{aligned} K_{M_1} &= \frac{K_E K_M}{R} \\ K_{M_2} &= \frac{K_M}{R}. \end{aligned} \tag{21}$$

It must be noted that as the rotor is fixed to the drive shaft of the motor, $\omega_M = \omega$ in Eq. 20.

To complete the actuator dynamics model, the thrust produced by the rotor is calculated as follows:

$$\begin{aligned} T &= \rho A \omega^2 R^2 C_T \\ &= \rho c R^3 B^2 \omega^2 C_{L_\alpha} \left(\frac{\alpha_0 B}{3} - \frac{V_i}{2R\omega}\right). \end{aligned} \tag{22}$$

Eq. 22 is further simplified into the following equation:

$$T = K_{T_1} \omega^2 \alpha_0 - K_{T_2} \omega, \tag{23}$$

where

$$\begin{aligned} K_{T_1} &= \frac{1}{3} \rho c R^3 B^3 C_{L_\alpha} \\ K_{T_2} &= \frac{1}{2} \rho c R^2 B^2 V_i C_{L_\alpha}. \end{aligned} \tag{24}$$

Eq. 20 and Eq. 23 make up the complete nonlinear actuator dynamics model.

2.3 Control Allocation of Variable-Pitch Rotors

Inspection of Eq. 20 and Eq. 23 reveals two available control inputs into the dynamics model of variable-pitch rotor systems: the voltage applied to the motor, v, and the rotor blade angle, α_0. Similar to [11], the dynamics model of the variable-pitch rotor system can be linearised about the hover condition, $\omega = \omega_H$ and $\alpha_0 = \alpha_{0,H}$.

$$\begin{aligned} \Delta\dot{\omega} &= \left[-\frac{K_{M_1}}{I_{TM}} - \frac{2K_{Q_1}\omega_H \alpha_{0,H}}{I_{TM}} - \frac{2K_{Q_2}\omega_H}{I_{TM}} - \frac{K_{Q_3}\alpha_{0,H}}{I_{TM}} \right] \Delta\omega \\ &\quad + \left[\frac{K_{M_2}}{I_{TM}} - \frac{2K_{Q_1}\omega_H^2 \alpha_{0,H}}{I_{TM}} - \frac{K_{Q_3}\omega_H}{I_{TM}} \right] \begin{bmatrix} \Delta v \\ \Delta\alpha_0 \end{bmatrix} \\ \Delta T &= \left[K_{T_1}\omega_H \alpha_{0,H} - K_{T_2} \right] \Delta\omega + \left[0 K_{T_1} \omega_H^2 \right] \begin{bmatrix} \Delta v \\ \Delta\alpha_0 \end{bmatrix} \end{aligned} \tag{25}$$

The output of the dynamics system is the change in thrust, ΔT, $\Delta\omega$ is an internal state of the system, and Δv and $\Delta\theta_0$ are the control inputs.

As discussed in [11], the linearised dynamics model demonstrates the fundamental difference between fixed-pitch rotors and variable collective-pitch rotors. If the pitch is held constant in the state-space model presented in Eq. 25, the thrust can only be actuated by first altering $\Delta\omega$ through applying Δv: the Δv control input only affects the ΔT output through the motor dynamics. If the pitch of the rotor is free to vary, there exists a direct feed-through term in the output equation: the $\Delta\alpha_0$ control input bypasses the motor dynamics.

However, a complication arises in that altering the pitch of the rotor negatively affects the angular velocity of the motor due to an increase in load torque (16). To overcome this, it is necessary to incorporate a control architecture into the system that responds quickly

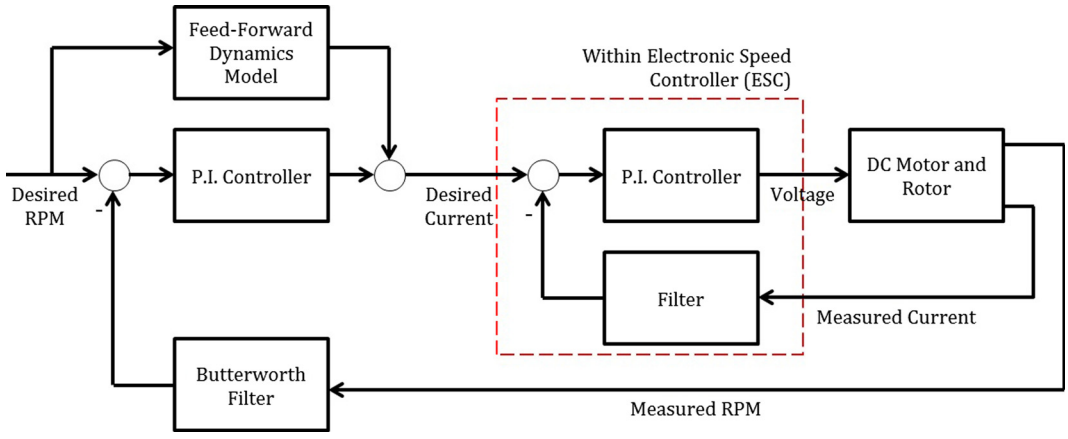

Fig. 2 The proposed rotor angular velocity feedback control architecture

to changes in motor load torque and rotor angular velocity.

The proposed rotor angular velocity control architecture is presented in Fig. 2. The feed-forward dynamics model is derived from the inversion of Eq. 20 in the steady state ($\dot{\omega} = 0$). Here, it is necessary to calculate v/R rather than v, as the input to the Electronic Speed Controller (ESC) is the desired motor current draw. The feed-forward model is presented in Eq. 26. The *PI* Controller in Fig. 2 is a common automatic control technique and is discussed in most control texts (see for example, [3]). The ESC measures the angular velocity of the motor via a flux-observer. A 5th-order low-pass Butterworth Filter is applied to this output to attenuate any sensor noise. The cutoff frequency of the Butterworth Filter, f_c, is set at $f_c/f_0 = 0.22$, where the sample frequency, f_0, is 1000Hz. The cutoff frequency was chosen to attenuate noise above the maximum expected rotor angular velocity of 13000RPM. The order of the Butterworth Filter was calculated to achieve a desired attenuation of 20dB at 300Hz.

$$\frac{v}{R} = \frac{1}{RK_{M_2}}(K_{M_1}\omega + K_{Q_1}\omega^2\alpha_0^2 + K_{Q_2}\omega^2 + K_{Q_3}\omega\alpha_0 + K_{Q_4}) \tag{26}$$

The control architecture presented in Fig. 2 allows the angular velocity of the rotor to be set independently of the rotor blade pitch angle. The varying

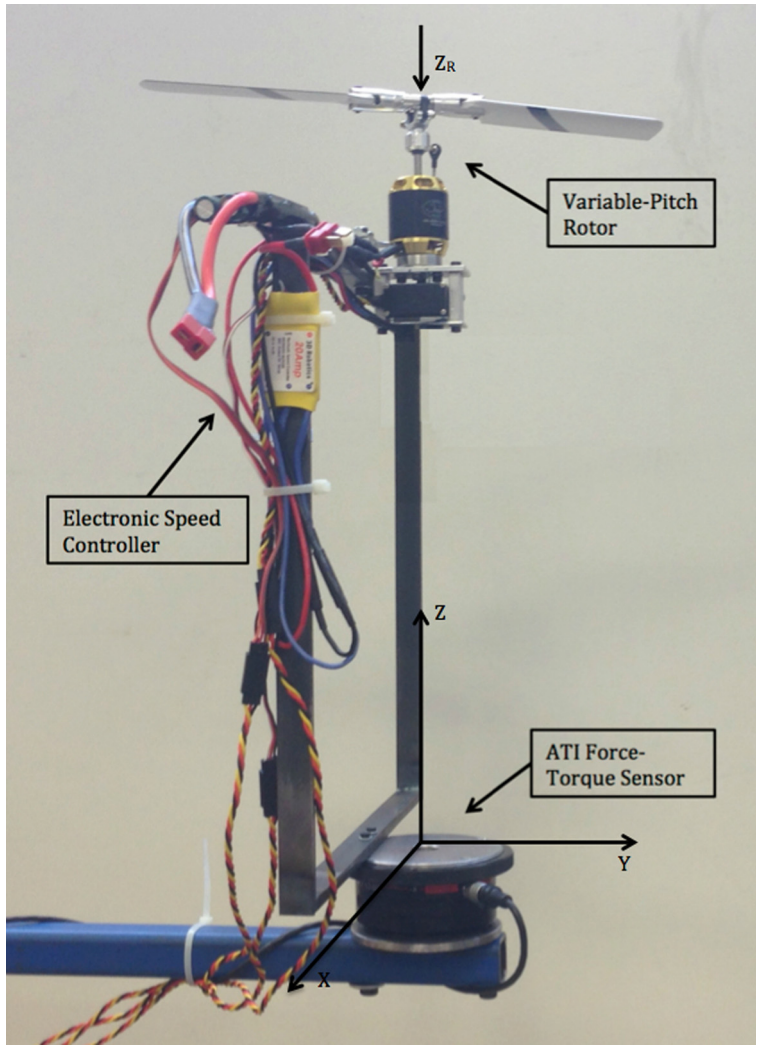

Fig. 3 The rotor thrust-torque experimental platform

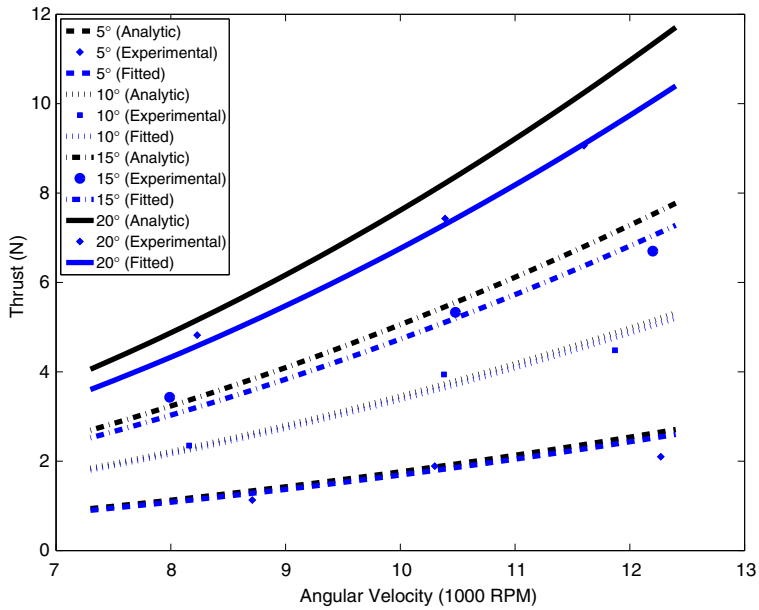

Fig. 4 Steady state thrust versus rotor angular velocity as a function of rotor blade angle of attack

motor load torque due to the rotor blade angle of attack is compensated for by the feedback control loop.

3 Experimental Model Verification

In this section an experimental analysis of the motor and rotor dynamics is undertaken. To this end, an experimental platform incorporating a six-axis force-torque sensor has been developed. In designing the experimental platform, care has been taken to minimise ground effect by ensuring the rotor downwash is unencumbered as possible. The experimental platform is presented in Fig. 3.

The force-torque sensor is able to measure forces within the range of $\pm 80N$ with a resolution of $0.02N$

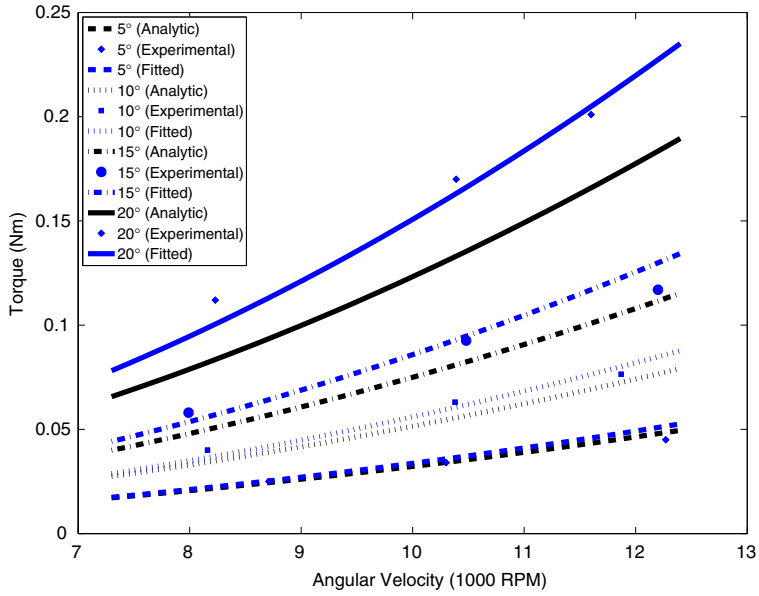

Fig. 5 Steady state torque versus rotor angular velocity as a function of rotor blade angle of attack

along the X and Y axes, and $\pm 240N$ with a resolution of $0.04N$ along the Z axis. The sensor is able to measure torques within the range of $\pm 4Nm$ with a resolution of $0.0005Nm$ about all X, Y and Z axes. The force-torque sensor is capable of a sampling rate of up to 500Hz. The sampling rate depends on the number of axes the of forces and torques being measured.

The experimental platform also incorporates an ammeter and voltmeter that are able to record measurements at a rate of 100Hz. This allows the power consumption of the motor to be calculated.

3.1 Steady State Response of Actuators

The rotor was initially driven without the closed-loop control scheme. Instead, inputs to the ESC were given directly and the resulting rotor angular velocities were recorded. This allowed the thrust and torque produced by the rotor to be measured as a function of rotor angular velocity and rotor blade angle of attack. The results of this experiment are presented in Figs. 4 and 5. In these figures, the continuous experimental results are obtained through post-processing the discrete data points.

The results obtained from the experimental analysis demonstrate good agreement with the analytic predictions made in Section 2.1. For higher blade angles of attack, the analytically derived model over-predicts the measured thrust values by as much as 15 %. This is likely due to the flow over the rotor blade beginning to separate from the blade, violating the laminar flow assumption made in the analytic derivation. This is further supported by the significant increase in torque load over the analytic results as the rotor blade angle of attack increases.

Table 2 Experimental torque load coefficients

$K_{Q_1}\ (Kg.m^2)$	$K_{Q_2}\ (Kg.m^2)$
$1.20e{-}06$	$6.15e{-}09$
$K_{Q_3}\ (Kg.m^2/s)$	$K_{Q_4}\ (Kg.m^2/s^2)$
$-1.19e{-}04$	$3.06e{-}02$

The experimental torque load results allow the coefficients in Eq. 18 to be calculated using least-squares regression. These calculated coefficients are presented in Table 2.

3.2 Actuator Power Consumption

Throughout the experiments presented in Section 3.1, the voltage supplied to the motor and the current drawn by the motor were recorded. This allows the power consumption of the actuator to be calculated.

In Fig. 6, the thrust produced by the variable collective-pitch rotor is plotted against the actuator power consumption for various rotor blade angles of attack. This provides an insight into operating

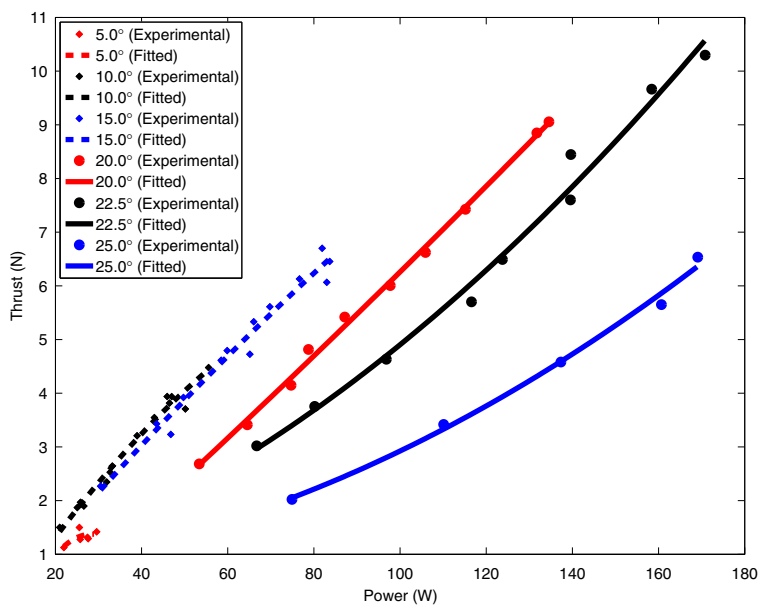

Fig. 6 Steady state thrust response versus power consumption as a function of rotor blade angle of attack

Table 3 Experimental motor coefficients

K_{FF_1} $(A.s)$	F_{FF_2} (A/Nm)
$4.43e{-}04$	$7.02e{-}03$

regimes for variable-pitch rotor equipped multirotor helicopters if the objective is to conserve as much energy as possible. For example, the power consumption can be reduced significantly by ensuring the rotor blade angle of attack remains under 15 degrees if the desired thrust is less than $6N$. This can be achieved by varying the motor angular velocity rather than the rotor blade angle of attack if the response time of the system can be maintained below the $0.2s$ threshold as discussed in [23].

The results in Fig. 6 also demonstrate that the flow over the rotor blade has fully separated for a rotor blade angle of attack of 25 degrees. The flow separation results in an increased power consumption due to the increase in drag associated with flow separation. A significant decrease in thrust is also observed.

The remaining unknown coefficients in Eq. 26 can be calculated using the current drawn by the motors during the actuator power consumption experimental analysis. Eq. 26 can be rearranged into the following form

$$\frac{v}{R} = K_{FF_1}\omega + K_{FF_2}Q_L, \tag{27}$$

where

$$K_{FF_1} = \frac{K_{M_1}}{RK_{M_2}} = \frac{K_E}{R}$$
$$K_{FF_2} = \frac{1}{RK_{M_2}} = \frac{1}{K_M}. \tag{28}$$

The above allows the use of least squares regression to find K_{FF_1} and K_{FF_2}. The calculated coefficients are presented in Table 3.

3.3 Dynamic Response of Actuators

The most significant theoretical advantage of utilising variable collective-pitch rotors is the decreased thrust response time. In order to explore this performance advantage, the dynamic response of the variable collective-pitch rotor was compared against the dynamic response of an 11x4.7 fixed-pitch rotor. The 11x4.7 fixed-pitch rotor was chosen as the range of thrusts it is able to produce is comparable to the variable collective-pitch rotor for a similar range of rotor angular velocities. It is also very commonly utilised for multirotor helicopter applications.

Eq. 25 suggests that the thrust can be altered much more rapidly for a larger angular velocity, as $\Delta T \propto \omega_H^2 \Delta\theta_0$. Therefore, the affect the rotor angular velocity has on the response time for the variable collective-pitch rotor will also be explored.

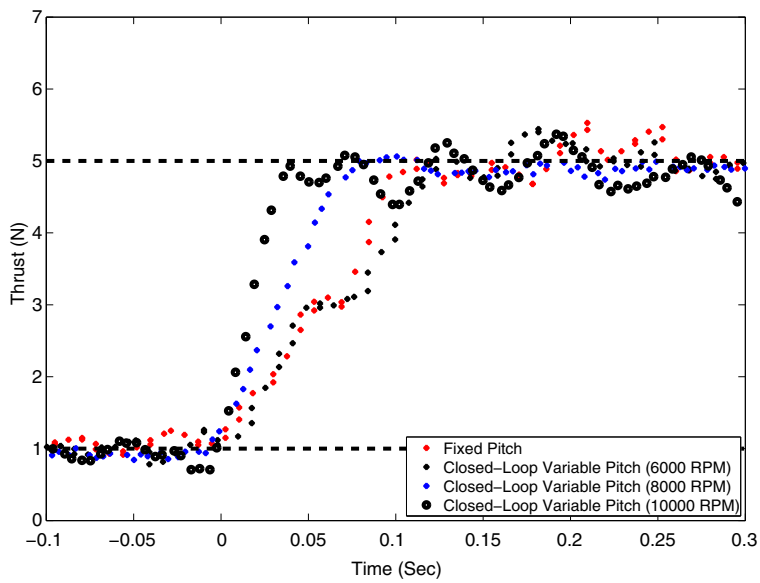

Fig. 7 Ascending step input response of actuators

The dynamic response of the rotors is characterised using both an ascending and descending step input. The ascending and descending step inputs are applied to the system independently after ensuring the rotor has reached a steady angular velocity. The results of applying an ascending and descending step input to the rotors are presented in Figs. 7 and 8, respectively. The closed-loop control scheme presented in Section 2.3 was used for both the variable collective-pitch rotor and the fixed-pitch rotor. The coefficients in the feed-forward model had to be experimentally determined individually for each rotor type.

For the ascending step input presented in Fig. 7, the fixed-pitch rotor has a settling time of $0.10s$. This is comparable to the variable-pitch rotor at an angular velocity of $6,000RPM$, which has a settling time of $0.12s$. However, the response time of the variable-pitch rotor improves significantly over the response time of the fixed-pitch rotor as the angular velocity of the variable-pitch rotor is increased: with an angular velocity of $8,000RPM$, the settling time is $0.075s$; an angular velocity of $10,000RPM$ results in a settling time of $0.04s$.

The performance of the fixed-pitch rotor suffered significantly for the descending step response, having a settling time of $0.3s$ (Fig. 8). This was as expected as Eq. 25 indicates that increasing the thrust produced by a fixed-pitch rotor is achievable by increasing the voltage. However, decreasing the thrust produced saturates the available control input as a negative voltage cannot be applied to the motor by the ESC.

The responses of the variable-pitch rotor to the descending step input are similar to the ascending step input responses. Only the variable-pitch rotor at $6000RPM$ demonstrated a significant difference in response, with the settling time reduced to $0.10s$. This is due to the servo having to apply less torque to overcome the load when decreasing the blade angle of attack compared to increasing the blade angle of attack. The change in load on the servo is due to the aerodynamic moment of the blade aiding the servo when decreasing the blade angle of attack [10]. This effect is less significant as the rotor angular velocity increases, as the blade angle of attack has to be altered by a lesser magnitude.

The experimental analysis has demonstrated a maximum potential improvement in response time of 60 % when using variable collective-pitch rotors over fixed-pitch rotors for an ascending step input response. For a descending step input response, the performance advantage is even more significant, with an improvement in response time of 87 % when using variable collective-pitch rotors.

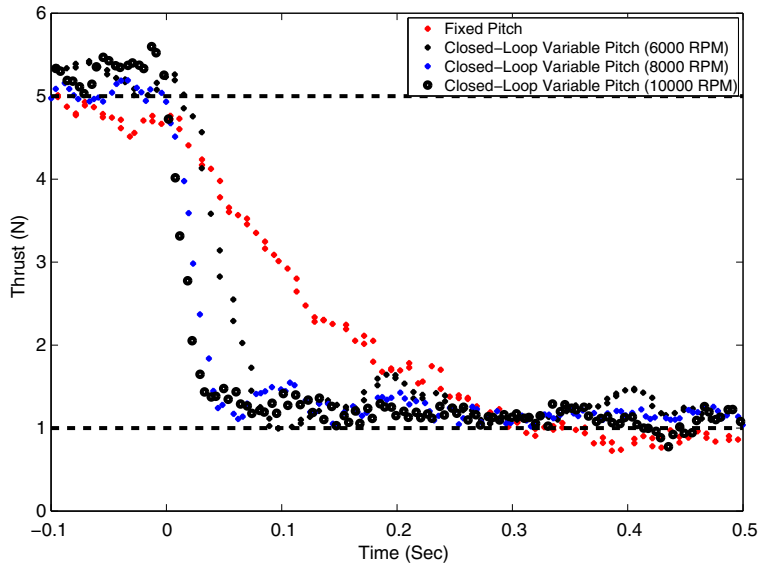

Fig. 8 Descending step input response of actuators

4 Experimental Analysis of the Effect of Actuators on Multirotor Helicopter Performance

4.1 Effect of Control Bandwidth on Multirotor Helicopter Response

In Section 3, an experimental analysis of variable-pitch rotors was undertaken. Variable-pitch rotors were found to have an increased maximum absolute thrust rate of change over fixed-pitch rotors of similar specification. The effect the enhanced bandwidth has on the flight performance of multirotor helicopters will be analysed in the following section.

To analyse the effect of enhanced bandwidth for multirotor helicopter applications, an experimental research facility has been established. The experimental facility consists of a quadrotor helicopter, a single degree of freedom (1DOF) test stand, and a high speed camera capable of recording 150 frames per second. The high speed camera utilised in conjunction with image processing software developed in MATLAB®allows a step input response in the attitude of the multirotor to be recorded and analysed. Vision-based ground-truth measurement and tracking is well established in research endeavours in a wide range of fields [9, 26]. The camera and image processing software is outside of the control loop of the quadrotor helicopter, which relies on the Madgwick Attitude Determination Algorithm [17] for attitude state estimation. Previous research undertaken by the authors has confirmed the suitability of the Madgwick Attitude Determination Algorithm for UAV application [8].

A still image taken using the high-speed camera during the experimental analysis is presented in Fig. 9.

The attitude of the quadrotor helicopter is regulated using the feedback control architecture presented in Fig. 10. Here, the output of the PID Controller, U_D, is the desired moment about the centre of gravity of the quadrotor. The control allocation block calculates the thrust required of each rotor using the algorithm presented in Eq. 29, and determines the appropriate rotor blade pitch angle and rotor angular velocity using Eq. 25. The motor angular velocity is regulated using the control architecture presented in Section 2.

$$\begin{bmatrix} \theta_{0,L} \\ \theta_{0,R} \end{bmatrix} = \frac{1}{2K_{T,1}\omega^2} \begin{bmatrix} -\frac{1}{D} & 1 \\ \frac{1}{D} & 1 \end{bmatrix} \begin{bmatrix} U_D \\ T_{total} \end{bmatrix} \tag{29}$$

In Eq. 29, the subscripts L and R indicate the left and right rotor, respectively, D is the distance between the centres of the two rotors, T_{total} is the total desired thrust produced by the two rotors. T_{total} is set at 1.5 times the total weight (N) of the quadrotor helicopter for this analysis.

In Section 3.3 it was demonstrated that higher rotor angular velocities increase the available actuator control bandwidth. Therefore, the rotor angular velocities are held at $10,000 RPM$ for the following

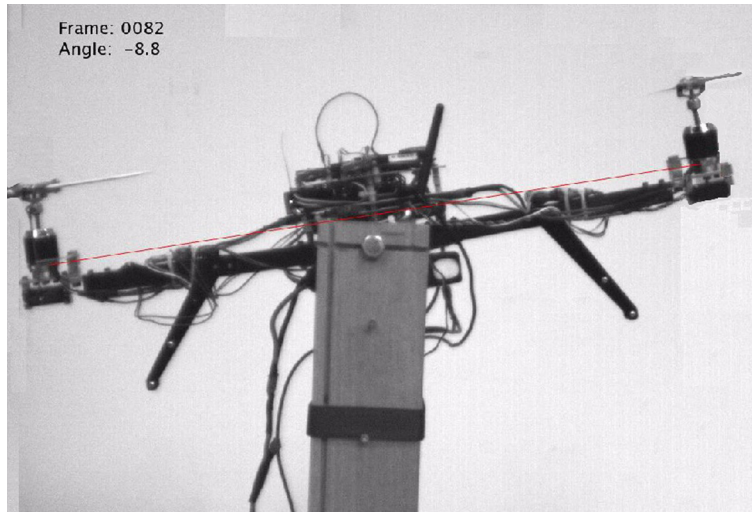

Fig. 9 A still image of the multirotor helicopter on the 1DOF test stand

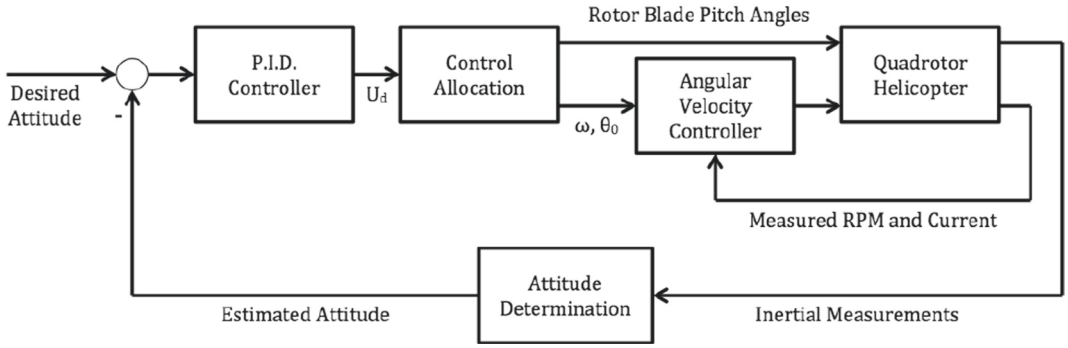

Fig. 10 The attitude PID feedback control

experimental analysis. This corresponds to the highest rotor angular velocity that could be achieved without inducing unmanageable vibration of the quadrotor helicopter.

The experimental procedure adopted is as follows. Using the variable-pitch rotors, the Ziegler-Nichols (ZN) PID controller tuning methodology is utilised. That is, the integral and derivative gains of the PID controller, K_I and K_D respectively, are set to zero and the proportional gain, K_P, is increased until an impulse control input induces a constant amplitude oscillation of the quadrotor helicopter. At this point K_P is recorded as the ultimate gain, K_U. The period of constant-amplitude oscillation, T_U, is determined by applying a Fast Fourier Transform (FFT) to the recorded ground-truth attitude. The PID controller gains are then set using the tuning guide presented in Table 4 [19]. Once the PID controller gains have been determined using the Ziegler-Nichols tuning methodology, the step response for each of the tuning gains is recorded. The entire process is repeated using fixed-pitch rotors on the quadrotor helicopter.

Although the above-mentioned method of tuning the PID Controller is unlikely to result in optimal performance [19], it does allow the variable-pitch rotor equipped quadrotor to be compared to the fixed-pitch rotor equipped quadrotor for a given set of PID parameters. This allows conclusions to be drawn regarding the performance of the quadrotor due to enhanced actuator bandwidth.

The step-input results are presented for the variable-pitch rotors in Fig. 11, and for the fixed-pitch rotors in Fig. 12. The rise time, settling time and percentage overshoot are given for each set of rotors and for each tuning methodology in Table 5.

The results in Table 5 provide a clear indication of how the enhanced control bandwidth available due to the utilisation of variable collective-pitch rotors improve the agility of the quadrotor helicopter. The fixed-pitch rotor equipped quadrotor demonstrates an average increase in rise time of 21 %, an average of 12 % increase in settling time, and has an average of 9 % greater percentage overshoot over the same quadrotor fitted with variable collective-pitch rotors.

Table 4 PID control tuning rules

Tuning rule	K_P	K_I	K_D
P	$0.5K_U$		
PI	$0.45K_U$	$1.2K_P/T_U$	
PD	$0.8K_U$		$0.125K_PT_U$
ZN PID	$0.6K_U$	$2K_P/T_U$	$0.125K_PT_U$
Pessen integral rule	$0.7K_U$	$0.4K_P/T_U$	$0.15K_PT_U$
Some overshoot	$0.33K_U$	$2K_P/T_U$	$0.33K_PT_U$

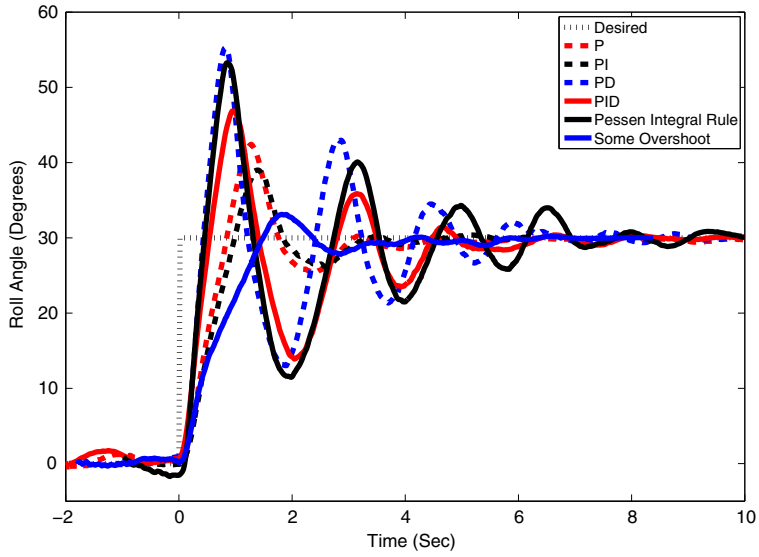

Fig. 11 Step input response of the variable collective-pitch rotor equipped quadrotor

4.2 Power Consumption during Smooth Trajectory Tracking

An important consideration for actuators for use in multirotor helicopter applications is the effect they have on the power consumption of the system. To this end, the power consumption of the quadrotor helicopter when utilising fixed-pitch rotors and variable collective-pitch rotors will be analysed under expected-use conditions. To simulate expected-use conditions, the quadrotor helicopter is made to track a smooth sinusoidal attitude trajectory for $200s$ using each set of rotors. The current drawn by the quadrotor helicopter, and the voltage supplied to the quadrotor helicopter are recorded at a rate of $100Hz$ throughout the trajectory tracking.

The attitude PID feedback controller was tuned using the *ZN PID* tuning rule for this experiment. This

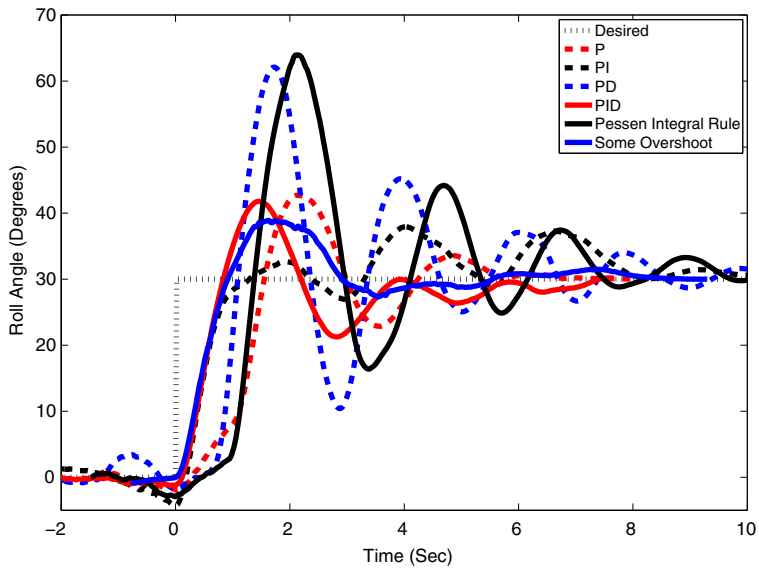

Fig. 12 Step input response of the fixed collective-pitch rotor equipped quadrotor

Table 5 Multirotor step input response characteristics

Tuning rule	Characteristic	Variable-Pitch	Fixed-Pitch
P	Rise time	0.58s	1.01s
	Overshoot	41 %	43 %
	Settling time	6.1s	9.69s
PI	Rise time	0.70s	0.74s
	Overshoot	21 %	30 %
	Settling time	3.32s	11.61s
PD	Rise time	0.27s	2.02s
	Overshoot	85 %	109 %
	Settling time	15.80s	17.02s
ZN PID	Rise time	0.38s	0.53s
	Overshoot	56 %	39 %
	Settling time	7.76s	7.80s
Pessen integral rule	Rise time	0.25s	0.38s
	Overshoot	77 %	113 %
	Settling time	8.63s	12.60s
Some overshoot	Rise time	1.13s	0.65s
	Overshoot	10 %	30 %
	Settling time	5.42s	6.76

tuning rule was chosen as the step input response of the quadrotor helicopter was similar when using either set of rotors (Table 5).

The results obtained during the experimental analysis are presented in Fig. 13. In this figure, the motors are set to an idle angular velocity at approximately $-10s$, and the smooth trajectory tracking begins at time $0s$.

The total power consumption for the first $200s$ of smooth trajectory tracking was $500mAh$ for the quadrotor equipped with fixed-pitch rotors, and $402mAh$ for the quadrotor equipped with

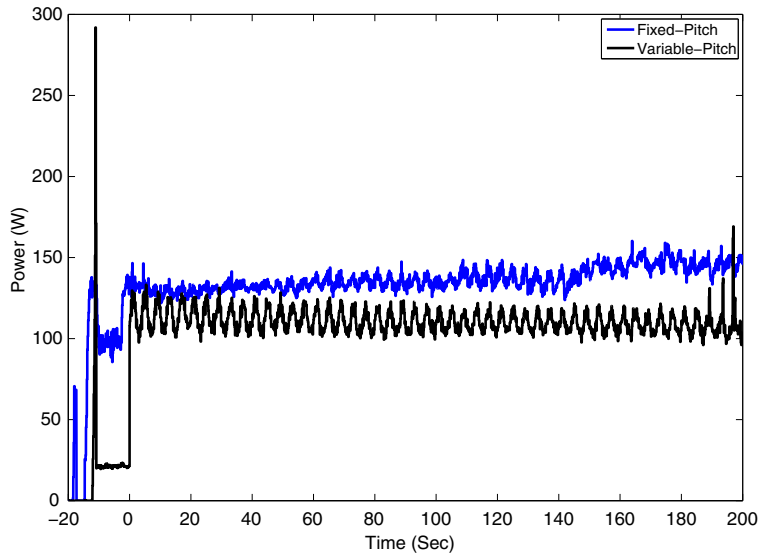

Fig. 13 Quadrotor power consumption during sinusoidal attitude trajectory tracking

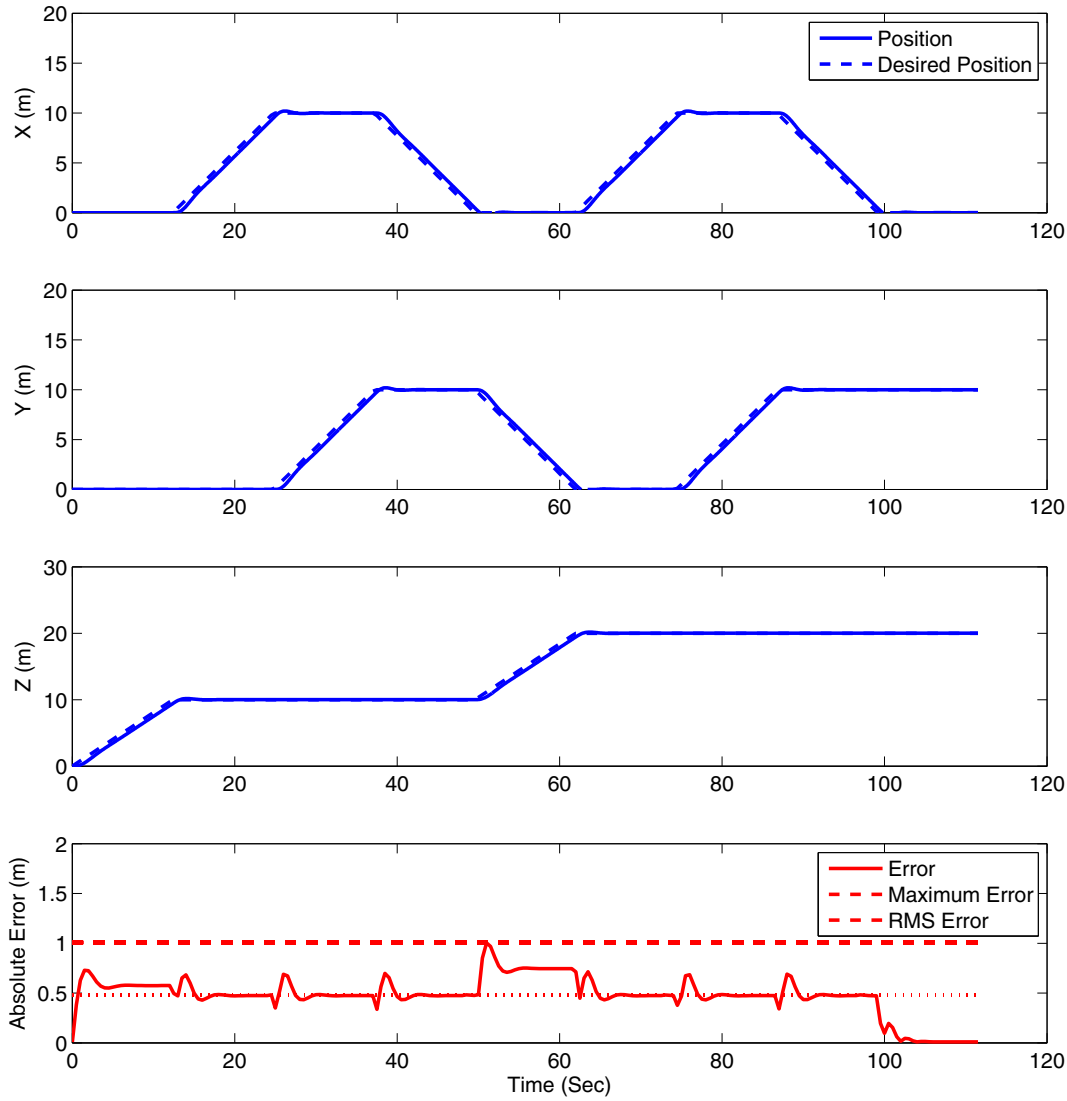

Fig. 14 Smooth trajectory tracking of fixed collective-pitch rotor equipped quadrotor

variable-pitch rotors. Therefore, the variable-pitch rotors reduce the overall power consumption of the system by 19.6 %.

5 Computational Analysis of Variable Collective-pitch Rotor-equipped Multirotor Helicopter Performance

To further explore the effect variable collective-pitch rotors have on multirotor helicopter performance, a computational analysis has been conducted. This analysis utilised the rotor parameters obtained in Section 3 within a multirotor helicopter computational model. The control scheme presented in Fig. 10 was utilised within the computational analysis, as were the *PI* PID control tunings found in Section 4.1. The dynamic and kinematic equations that make up the multirotor helicopter dynamics model are those widely described within multirotor helicopter literature (for example, [25]). A 4^{th}-order Runge-Kutta method was implemented to numerically solve the differential equations within the multirotor helicopter dynamics model.

To compare the performance between fixed collective-pitch rotors and variable collective-pitch rotors, two quadrotor helicopters were tasked with tracking a non-smooth 3-dimensional trajectory with a maximum allowable absolute error of $1.00m$. The first quadrotor helicopter was equipped with fixed collective-pitch rotors, and the second with variable collective-pitch rotors. The total time taken for each quadrotor to complete the desired trajectory allows for a comparison between rotor systems. To this end, the trajectory was parametrised in time and a line-search was conducted to find the minimum total time given the maximum allowable absolute error condition. The results of the analysis are presented in Figs. 14 and 15.

As presented in Fig. 14, the fixed collective-pitch rotor equipped quadrotor helicopter completed the trajectory tracking in $111.55s$. The quadrotor helicopter with variable-collective pitch rotors completed the trajectory tracking in $105.07s$, as presented in Fig. 15. This represents an improvement of 5.8 % when comparing variable collective-pitch rotors to fixed collective-pitch rotor systems.

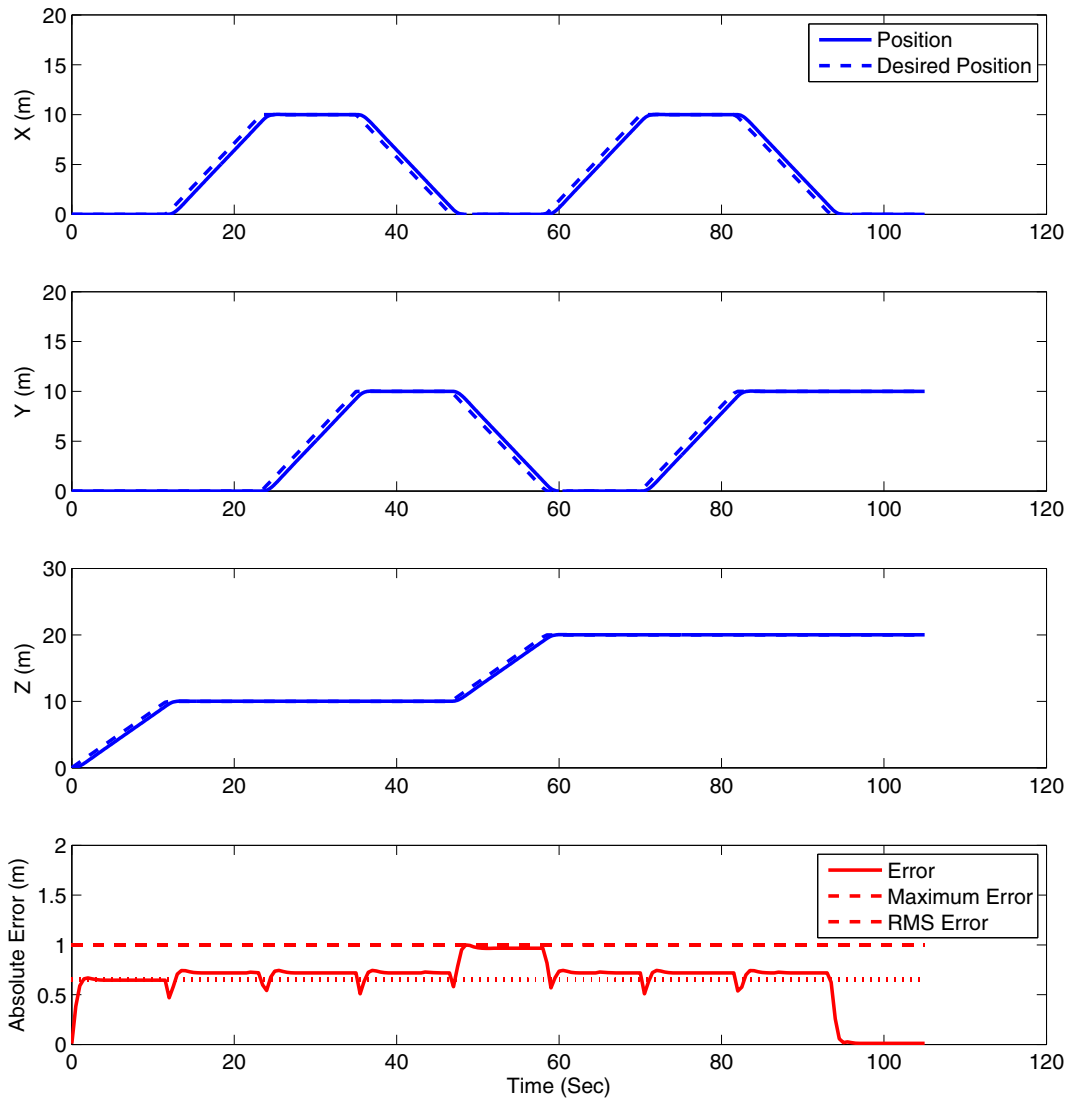

Fig. 15 Smooth trajectory tracking of variable collective-pitch rotor equipped quadrotor

6 Conclusions

This paper presented a detailed experimental analysis of variable collective-pitch rotors for multirotor helicopter application.

The dynamics models of the variable collective-pitch rotors and brushless DC motors were developed. This resulted in a full nonlinear dynamics model of the rotor and motor system. The dynamics model was utilised to establish a rotor angular velocity feedback control architecture, allowing the rotor angular velocity to be controlled in the presence of changing load torque on the motor.

Further, an experimental analysis of variable collective-pitch rotors was conducted to characterise the performance of the system in comparison to fixed-pitch rotor systems. The performance of a quadrotor helicopter was also investigated when equipped with both fixed-pitch rotors and variable collective-pitch rotors.

The experimental analysis demonstrated a clear performance advantage when utilising variable collective-pitch rotors in place of fixed-pitch rotors for multirotor helicopter applications. This performance advantage was primarily in the response time, and therefore agility, of multirotor helicopters. A secondary benefit of utilising variable collective-pitch rotors was the reduction in power consumption of the multirotor system. A computational analysis further demonstrated that the performance advantage of variable collective-pitch rotors translated to improved flight performance of multirotor helicopters.

The performance advantage does come at the cost of increased mechanical complexity, however this is minimised by avoiding the use of swashplates found in traditional pod-and-boom helicopters. It is therefore concluded that incorporating variable collective-pitch rotors for multirotor helicopter application is a viable option when developing multirotor helicopters capable of agile flight regimes.

Future work will continue to explore the performance advantages of equipping multirotor helicopters with variable collective-pitch rotor systems.

Acknowledgments This work was supported in part by ARC LIEF-R001078/82, ARC LIEF-LE0347024, ARC LIEF-LE0775692 and ARC Linkage-LP0668052.

References

1. Abbeel, P., Coates, A., Quigley, M., Ng, A.Y.: An application of reinforcement learning to aerobatic helicopter flight. Adv. Neural Inf. Process. Syst. **19**, 1 (2007)
2. Alaimo, A., Artale, V., Milazzo, C.L.R., Ricciardello, A.: PID controller applied to hexacopter flight. J. Intell. Robot. Syst. **73**(1-4), 261–270 (2014)
3. Astrom, K.J., Hagglund, T.: PID controllers: theory, design, and tuning, 2 edn. Instrument Society of America. Research Triangle Park, NC (1995)
4. Borenstein, J.: The hoverbot - an electrically powered flying robot (1992)
5. Bošnak, M., Matko, D., Blažič, S.: Quadrocopter hovering using position-estimation information from inertial sensors and a high-delay video system. J. Intell. Robot. Syst. **67**(1), 43–60 (2012)
6. Bouabdallah, S., Noth, A., Siegwart, R.: PID vs LQ control techniques applied to an indoor micro quadrotor. In: Proceedings of the IEEE/RSJ International Conference on Intelligent Robots and Systems, 2004, vol. 3, pp. 2451–2456 (2004)
7. Bresciani, T.: Modelling, identification and control of a quadrotor helicopter. Unpublished masters thesis, Lund University, Lund, Sweden (2008)
8. Choi, M.H., Porter, R., Shirinzadeh, B.: Comparison of attitude determination methodologies for implementation with 9DOF, low cost inertial measurement unit for autonomous aerial vehicles. Int. J. Intell. Mechatron. Robot. **3**(2), 1–15 (2013)
9. Clark, L., Shirinzadeh, B., Tian, Y., Oetomo, D.: Laser-based sensing, measurement, and misalignment control of coupled linear and angular motion for ultrahigh precision movement. IEEE/ASME Trans. Mechatron. **20**(1), 84–92 (2015)
10. Cook, M.V. Flight Dynamics Principles: A Linear Systems Approach to Aircraft Stability and Control, 2nd. Elsevier Aerospace Engineering Series. Butterworth-Heinemann, Great Britain (2007)
11. Cutler, M., Ure, N.K., Michini, B., How, J.P.: Comparison of fixed and variable pitch actuators for agile quadrotors. In: AIAA Guidance, Navigation, and Control Conference (2010)
12. Gavrilets, V., Frazzoli, E., Mettler, B., Piedmonte, M., Feron, E.: Aggressive maneuvering of small autonomous helicopters: A human-centered approach. Int. J. Robot. Res. **20**(10), 795–807 (2001)
13. Hooper, R.: 3D-printing drone squirts foam to pick up waste. New Sci. **222**(2968), 21 (2014)
14. Kuethe, A., Chow, C.Y. Foundations of Aerodynamics, 5th edn. Wiley, New York (1998)
15. Lee, D.J., Kaminer, I., Dobrokhodov, V., Jones, K.: Autonomous feature following for visual surveillance using a small unmanned aerial vehicle with gimbaled camera system. Int. J. Control Autom. Syst. **8**(5), 957–966 (2010)
16. Leishman, J.G.: Principles of helicopter aerodynamics. Cambridge Aerospace Series, Cambridge University Press, New York (2006)

17. Madgwick, S.O., Harrison, A.J., Vaidyanathan, R.: Estimation of imu and marg orientation using a gradient descent algorithm. In: IEEE International Conference on Rehabilitation Robotics, 2011, pp. 1–7. IEEE (2011)
18. Mahony, R., Kumar, V., Corke, P.: Multirotor aerial vehicles: Modeling, estimation, and control of quadrotor. IEEE Robot. Autom. Mag. **19**(3), 20–32 (2012)
19. McCormack, A.S., Godfrey, K.R.: Rule-based autotuning based on frequency domain identification. IEEE Trans. Control Syst. Technol. **6**(1), 43–61 (1998)
20. Mellinger, D., Michael, N., Kumar, V.: Trajectory generation and control for precise aggressive maneuvers with quadrotors. Int. J. Robot. Res. **31**(5), 664–674 (2012)
21. Orsag, M., Cesic, J., Haus, T., Bogdan, S.: Spincopter wing design and flight control. J. Intell. Robot. Syst. **70**(1-4), 165–179 (2013)
22. Pestana, J., Mellado-Bataller, I., Sanchez-Lopez, J.L., Fu, C., Mondragón, I.F., Campoy, P.: A general purpose configurable controller for indoors and outdoors gps-denied navigation for multirotor unmanned aerial vehicles. J. Intell. Robot. Syst. **73**(1-4), 387–400 (2014)
23. Pounds, P., Mahony, R.: Design principles of large quadrotors for practical applications. In: IEEE International Conference on Robotics and Automation, 2009, pp. 3265–3270
24. Tan, R., Kumar, M.: Tracking of ground mobile targets by quadrotor unmanned aerial vehicles. Unmanned Syst. **02**(02), 157–173 (2014)
25. Tayebi, A., McGilvray, S.: Attitude stabilization of a vtol quadrotor aircraft. IEEE Trans. Control Syst. Technol. **14**(3), 562–571 (2006)
26. Wang, X., Shirinzadeh, B.: High-order nonlinear differentiator and application to aircraft control. Mech. Syst. Signal Process. **46**(2), 227–252 (2014)
27. Wang, X., Shirinzadeh, B.: Nonlinear multiple integrator and application to aircraft navigation. IEEE Trans. Aerosp. Electron. Syst. **50**(1), 607–622 (2014)